



Evaluation of phosphate adsorption by porous strong base anion exchangers having hydroxyethyl substituents: kinetics, equilibrium, and thermodynamics

Doina Humelnicu¹ · Ecaterina Stela Dragan²

Received: 27 July 2020 / Accepted: 21 September 2020 / Published online: 6 October 2020
© Springer-Verlag GmbH Germany, part of Springer Nature 2020

Abstract

Phosphate anions are recognized as the main responsible for the eutrophication of surface waters. In this work, two strong base anion exchangers having either N,N-dimethyl 2-hydroxyethylammonium (SBAEx.2M) or N,N-diethyl 2-hydroxyethylammonium (SBAEx.2E) functional groups, as highly efficient sorbents in the removal of phosphate anions, are presented. The influence of the main parameters (pH, contact time, initial concentration of phosphate, temperature) on the adsorption performances was investigated in batch mode. Modeling the kinetics data by Lagergren, Ho and McKay, and Elovich kinetic models indicated chemisorption as the main mechanism of sorption. The sorption at equilibrium was modeled with Langmuir, Freundlich, Sips, Dubinin-Radushkevich, and Temkin isotherm models. The experimental isotherms were the best fitted by Langmuir and Sips isotherms, the maximum sorption capacity for phosphate anions being 233.88 mg g⁻¹ SBAEx.2M and 223.5 mg g⁻¹ SBAEx.2E, at pH 3, and 23 °C. Adsorption of phosphate anions in competitive conditions showed that the interference with co-existing anions was low in the case of Cl⁻ ions and much higher with SO₄²⁻ ions, the ion exchange having an important contribution in the adsorption process. The adsorption was spontaneous and endothermic, the degree of spontaneity increasing with the increase of temperature. The high level of reusability, the adsorption capacity decreasing with only ~7% in the case of SBAEx.2E and with ~9% in the case of SBAEx.2M, after five sorption/desorption cycles, recommends these SBAEx as promising adsorbents for phosphate removal.

Keywords Phosphate · Strong base anion exchangers · Sorption kinetics · Isotherms · Reusability

Introduction

Accumulation of toxic anions such as phosphate into the water containing an excess of nutrients determines over growth of algae into water bodies. That constitutes a very serious issue because blue-green algae are toxic and block sunlight to enter into water and use oxygen necessary for the plants and animals in water (Azam et al. 2019; Bunce et al. 2018; Dragan and Dinu 2020; Kumar and Viswanathan 2018). Therefore,

the phosphate removal in water bodies is highly required. In this respect, the interest in finding efficient and reusable adsorbents for phosphate has lately known a spectacular increase. Various approaches for physico-chemical removal of phosphate have been inspected, such as membrane processes (Zhao and Chen 2016), chemical precipitation (Nassef 2012), biological treatment (Bassin et al. 2012), and adsorption techniques. Among these, adsorption seems friendly with the environment and easier to operate compared with the other techniques (Dragan and Dinu 2020; Ye et al. 2019). The most investigated sorbents for their performances in phosphate removal could be grouped in (1) biomass-derived sorbents (Karthikeyan et al. 2019; Mahaninia and Wilson 2016, 2017), (2) inorganic oxides (Hao et al. 2019; Jing et al. 2020; Liu et al. 2011; Wu et al. 2019), (3) composite sorbents (Dragan et al. 2019; Du et al. 2020; Jia et al. 2020; Li et al. 2019; Liao et al. 2020; Luo et al. 2018, 2019; Rashid et al. 2017; Wan et al. 2017; Zong et al. 2018), and (4) ion exchangers (Ding et al. 2012; Liao et al. 2020; Liu et al. 2013;

Responsible Editor: Tito Roberto Cadaval Jr

✉ Ecaterina Stela Dragan
sdragan@icmpp.ro

¹ Faculty of Chemistry, “Alexandru Ioan Cuza” University of Iasi, Carol I Bd. 11, 700506 Iasi, Romania

² “Petru Poni” Institute of Macromolecular Chemistry, Grigore Ghica Voda Alley 41 A, 700487 Iasi, Romania

Sowmya and Meenakshi 2014; Wei et al. 2015; Zarrabi et al. 2014; Zhu et al. 2017). Various ion exchangers have been evaluated for their sorption capacity of phosphate, either alone (Ding et al. 2012; Liao et al. 2020; Liu et al. 2013; Sowmya and Meenakshi 2014; Wei et al. 2015; Zarrabi et al. 2014) or as hybrids with metal salts (Zhu et al. 2017). It has been reported that strong base anion exchangers (SBAEx) constitute a convenient alternative for phosphate adsorption/recovery (Ding et al. 2012; Sowmya and Meenakshi 2014; Wei et al. 2015). To increase the adsorption performances of the ion exchangers in the removal of phosphate and nitrate, a special attention has been paid to the sorbent hydrophobicity because it was observed that the increase of the hydrophobic character of the sorbent could determine the increase of the sorbent selectivity for a certain anion (Bui et al. 2018). The structural characteristics of the ion exchangers beside the textural properties decide their sorption performances (Dragan et al. 1995; Sowmya and Meenakshi 2014). In the case of SBAEx based on styrene-divinylbenzene matrix, the hydrophobic/hydrophilic balance could be controlled either by the cross-linking degree or by the alkyl substituents at the quaternary ammonium salt groups. Having in mind that no previous studies about the correlation between the adsorption performances for phosphate anions of porous SBAEx containing N,N-dialkyl 2-hydroxyalkyl ammonium functional groups and the hydrophobicity of the alkyl substituents have been reported, the objectives of the present study were (i) synthesis and characterization of porous SBAEx, different by the alkyl substituents ($-\text{CH}_3$ or $-\text{C}_2\text{H}_5$); (ii) investigation of the influence of pH, sorbent dose, phosphate concentration and temperature on the sorption capacity, and removal efficiency in non-competitive conditions as a function of the alkyl substituents; (iii) to model the kinetic and equilibrium of phosphate adsorption in order to evaluate the kinetic and isotherm parameters and to discuss the adsorption mechanism; (iv) to evaluate the influence of interfering anions, such as Cl^- , NO_3^- , and SO_4^{2-} , on the phosphate adsorption capacity; and (v) to establish the level of reusability of the SBAEx during consecutive sorption/desorption cycles.

Materials and methods

Materials

Styrene (99% purity) (Arpechim, Romania) and DVB (54.5% o-DVB, m-DVB, p-DVB, 36.2% ethylstyrene, and 9.3% inert compounds) (Viromet Co., Romania) were distilled under reduced pressure before use. N-butyl alcohol (n-BA), chloroform, and methanol, purchased from Chemical Company, were used as received. Paraformaldehyde [$\text{HO}(\text{CH}_2\text{O})_n\text{H}$], FeCl_3 , and trimethyl chlorosilane (TMCS) (Fluka Chemical Co., Buchs,

Switzerland) were used as received. N,N-dimethyl 2-hydroxyethyl amine (DMHEA) and N,N-diethyl 2-hydroxyethyl amine (DEHEA) (Fluka Chemical Co., Buchs, Switzerland) were distilled under reduced pressure before use. KH_2PO_4 purchased from Fluka, $(\text{NH}_4)_6\text{Mo}_7\text{O}_{24}\cdot 4\text{H}_2\text{O}$ from Sigma-Aldrich, and potassium antimony (III) tartrate hemihydrate from Sigma-Aldrich were used as received. NaCl , NaNO_3 , and Na_2SO_4 purchased from Chemical Company were used as received.

Preparation and characterization of anion exchangers

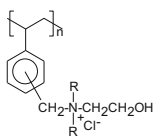
Synthesis of the SBAEx was performed following the previously presented protocol (Dragan et al. 2018). In brief, the synthesis of the ion exchangers used in this work consisted of three steps: (i) synthesis of the porous S-DVB copolymers in the presence of n-BA as porogen, (ii) chloromethylation to generate reactive groups, and (iii) amination with hydroxyalkyl tertiary amines. Only copolymers with 8% DVB were used in the synthesis of SBAEx. Chloromethylation was performed with a mixture of commercial $\text{HO}(\text{CH}_2\text{O})_n\text{H}$ and TMCS in the presence of FeCl_3 as catalyst. The amination was performed with DMHEA (for SBAEx.2M, Table 1) or DEHEA (for SBAEx.2E, Table 1), in DMSO, at 60 °C, 12 h, the mole ratio between amine and $-\text{CH}_2\text{Cl}$ being 2:1. The anion exchange capacity was determined after the sample regeneration with 1 M NaOH, values presented in Table 1.

For characterization in dry state, the samples were washed three times with methanol, dried in air 24 h, and under reduced pressure at 40 °C for 3 days. FT-IR spectra were recorded with a Bruker Vertex FT-IR spectrometer, resolution 2 cm^{-1} , in the range of $4000\text{--}400\text{ cm}^{-1}$ by the KBr pellet technique. The specific surface areas (S_{sp}) and pore size distribution were estimated from N_2 adsorption–desorption experiments conducted at 77 K using an Autosorb-1-MP surface area analyzer (Quantachrome Company, Boynton beach, FL, USA). The S_{sp} was estimated from the linear portion of the adsorption isotherms (0.05–0.35) by Brunauer–Emmett–Teller (BET) method.

Batch adsorption experiments

For the investigation of pH effect and for kinetics and equilibrium studies of phosphate adsorption in batch mode, the sorbent dose was 0.75 g L^{-1} . The experiments were performed in a water bath temperature-controlled shaker (GFL 1083, Gemini BV), vibrated at $\sim 160\text{ rpm}$. The effect of pH was examined over a pH range of 2.0–11.0, at 23 °C. The initial solution pH was adjusted with 1 M HCl or 1 M NaOH and was not controlled afterwards. For the study of the sorbent dose influence of the adsorption efficiency, the sorbent dose was varied in the range $0.5\text{--}5\text{ g L}^{-1}$, at pH 3, and a temperature

Table 1 Characteristics of the porous strong base anion exchangers tested for phosphate adsorption.

Functional group	Sorbent code	S_{sp} , $m^2 g^{-1}$	V_p , $cm^3 g^{-1}$	C_{sg} , $meq g^{-1}$
	R = CH ₃ , SBAEx.2M	3.968	0.0105 for pores with diameter < 46.9 nm	2.24
	R = C ₂ H ₅ , SBAEx.2E	46.686	0.0526 for pores with diameter < 48.7 nm	1.54

of 23 °C. Batch sorption of H₂PO₄⁻ ions as a function of contact time was performed using a solution of KH₂PO₄ with a concentration of 100 mg L⁻¹, at pH 3, at 23 °C, increasing time intervals from 15 to 1440 min. To investigate the sorption of H₂PO₄⁻ ions at equilibrium, the initial concentration of KH₂PO₄ was varied from 25 to 1000 mg L⁻¹, the phosphate concentration being determined after 24 h. After shaking for a certain time, the sorbent was separated from the metal ion solution by filtering through a 0.45-µm membrane filter. The concentration of phosphate ions in aqueous solution was determined by colorimetric method in the presence of ammonium molybdate and potassium antimonyl tartrate using ascorbic acid as reduction agent ($\lambda = 888$ nm), with a UV-Vis Hitachi U-2001 spectrophotometer (Nagul et al. 2015). Adsorption capacity at equilibrium, q_e (mg g⁻¹), was calculated based on mass balance, with Eq. 1:

$$q_e = \frac{(C_0 - C_e)V}{m} \tag{1}$$

where C_0 is the initial concentration of H₂PO₄⁻ ions (mg L⁻¹), C_e is the concentration of H₂PO₄⁻ ions in aqueous solution at equilibrium (mg L⁻¹), V is the volume of aqueous solution (L), and m is the weight of the dried sorbent (g).

The removal efficiency (RE) was evaluated with Eq. 2:

$$RE = \frac{C_0 - C_e}{C_0} \times 100 \tag{2}$$

where C_0 and C_e have the same meaning as in Eq. 1.

Desorption and reusability assays

To support the reusability of the SBAEx in the removal of phosphate anions in multiple sorption/desorption cycles, desorption test was carried out on the sorbents loaded with phosphate anions at a concentration of 100 mg L⁻¹, at 23 °C, at a contact time of 8 h and a stirring rate of 160 rpm. Desorption was performed with 4 wt.% NaCl aqueous solution. Then, the SBAEx samples were washed several times with distilled water and reused in another cycle up to five consecutive sorption/desorption cycles.

Results and discussion

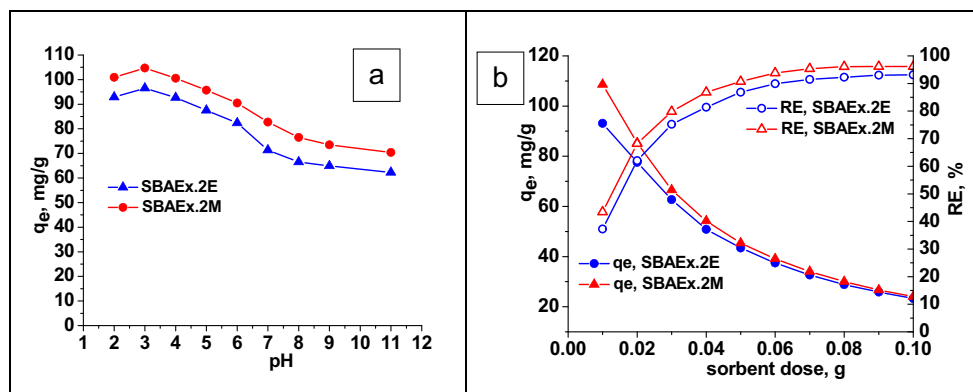
Effect of pH and sorbent dose

Figure 1 presents the influence of initial pH of phosphate aqueous solution (a) and of sorbent dose (b) on the sorption capacity of SBAEx.2M and SBAEx.2E. As Fig. 1a shows, the maximum sorption capacity is located at pH values in the range of 2–4, with a maximum at pH 3, for both sorbents as observed for other anion exchangers (Liu et al. 2013; Zhu et al. 2017). Ionic species present in solution are depending on the solution pH (Kumar and Viswanathan 2019; Rashid et al. 2017; Wan et al. 2017; Wu et al. 2019). Thus, at low pH, H₃PO₄ is dominant, being weakly bound on the positively charged adsorption sites of the SBAEx. Increasing the pH, the electrostatic interaction between H₂PO₄⁻ anions, which are the main species in moderate acidic pH, and positive surface charge of anion exchangers is the highest in this range (Luo et al. 2018). At pH > 4, the values of q_e monotonously decreased and remained almost constant at pH > 7.0.

The large domain of pH where the SBAEx effectively adsorbs phosphate anions in acidic range is explained by the presence of quaternary ammonium salt groups as working functional moieties. At pH > 7.0, the sorption capacity decreased with about 30%, because the OH⁻ ions in excess compete with phosphate anions, but remain almost constant after that. Luo et al. have reported the maximum sorption capacity for phosphate ions of magnetic zirconium alginate beads at pH 2, the sorption decreasing up to pH 7, and remaining almost constant after that (Luo et al. 2018). Sowmya and Meenakshi have found that the sorption capacity remained almost constant when the pH varied in the range 3.0–8.0 (Sowmya and Meenakshi 2014). Bui et al. have reported a maximum of phosphate adsorption at pH 4.0 (Bui et al. 2018).

Figure 1 b shows that increasing the sorbent dose conducted to the decrease of the adsorption capacity and to the increase of the RE up to about 100%, when sorbent dose increased from 0.01 to 0.1 g. The explanation is that the number of active sites of the adsorbent available for phosphate adsorption increased, while the amount of phosphate anions adsorbed per weight unit of sorbent decreased accordingly, because the number of phosphate anions in contact with the sorbent weight unit decreased with the increase of the sorbent

Fig. 1 a Effect of pH on the sorption capacity of phosphate anions onto the SBAEx: temperature 23 °C, sorbent dose 0.75 g L⁻¹, initial concentration of phosphate 100 mg L⁻¹. **b** Effect of sorbent dose on the sorption capacity and removal efficiency of phosphate anions by the SBAEx: pH = 3, temperature 23 °C, initial concentration of phosphate 100 mg L⁻¹, volume of phosphate solution was 20 mL



dose (Dragan et al. 2018; Karthikeyan et al. 2019; Luo et al. 2018; Wu et al. 2019).

Adsorption kinetics and isotherms

Adsorption kinetics

The effect of contact time on the phosphate adsorption onto SBAEx.2M and SBAEx.2E is presented in Fig. 2a. As Fig. 2a shows, the equilibrium of sorption is reached in about 150 min, for both anion exchangers.

Kinetics data were modeled with pseudo-first-order (PFO) kinetic model (Lagergren 1898), pseudo-second-order (PSO) kinetic model (Ho and McKay 1998), and Elovich model (Juang and Chen 1997) (the equations are included in Table 2).

The kinetic parameters obtained by non-linear fitting of the models are presented in Table 2. The values of R^2 , both for PFO and PSO kinetic modes, are comparable, but the values of the calculated sorption capacities are closer to the experimental values in the case of PFO kinetic model. This fact would indicate physisorption as the main mechanism of sorption. To decide which model should be considered as the most appropriate, Elovich model, which indicates the role of heterogeneity of the adsorbent surface and also supports chemisorption as possible mechanism of sorption, was fitted on the kinetic data. As can be seen, the values of R^2 for Elovich model are high (0.9122 and 0.9314), and this indicates chemisorption as possible mechanism of sorption (Liu et al. 2013; Sowmya and Meenakshi 2014; Wei et al. 2015).

The experimental data were also fitted with the Weber and Morris model (equation is given in Table 2) to obtain information about the contribution of intra-particle diffusion (IPD) (Weber and Morris 1963). Figure 2b shows that the plots of q_t vs $t^{0.5}$ for the sorption of phosphate anions onto the porous anion exchangers are three linear. The first straight line could involve the diffusion of phosphate ions through the boundary layer to the external surface of anion exchanger beads (film diffusion), and the second step, with lower constants, could be

assigned to IPD or pore diffusion (Dragan et al. 2019; Jia et al. 2020; Liao et al. 2020; Luo et al. 2019). In the case of SBAEx.2E, the first straight line passes through the origin, but the second line did not, and that means that the IPD was not the only rate-controlling factor of the adsorption process. In the last step, the sorption slowed down for both anion exchangers due to both the decrease of the free ions in solution and to the decrease of active site number within the composite sorbent. C_i term in the Weber and Morris equation gives information about the thickness of boundary layer, which means the larger the intercept, the greater the contribution of film diffusion in the rate-limiting step (Dragan et al. 2019; Jia et al. 2020; Luo et al. 2019). The values of k_{id} , C_i , and R^2 for the first and the second steps in Fig. 2b are presented in Table 2. The high values of R^2 for the two steps support the applicability of the IPD model at these sorbents.

Isotherms

The experimental isotherms for the sorption of phosphate anions onto the SBAEx.2M and SBAEx.2E are presented in Fig. 3a.

The shape of both isotherms, by their abrupt slope, indicates a high affinity of these anion exchangers for phosphate anions. The isotherm parameters obtained by fitting five isotherm models (Langmuir, Freundlich, Sips, Dubinin-Radushkevich, and Temkin) on the experimental data are presented in Table 3 (the equations of the isotherm models are also included in Table 3).

As can be seen, the data accurately obeyed both Langmuir and Sips isotherms, the values of R^2 , and χ^2 being comparable. Thus, the adsorption was monolayer and support chemisorption involving ion exchange. The maximum adsorption capacity given by the Langmuir isotherm was 233.88 mg g⁻¹ SBAEx.2M, and 223.5/g SBAEx.2E.

The D-R isotherm allows the evaluation of the sorption energy, which gives indication about the sorption mechanism (Ding et al. 2012; Dragan et al. 2019). The mean free energy of adsorption, E (kJ mol⁻¹), was evaluated from D-R isotherm constant, β , by Eq. 3:

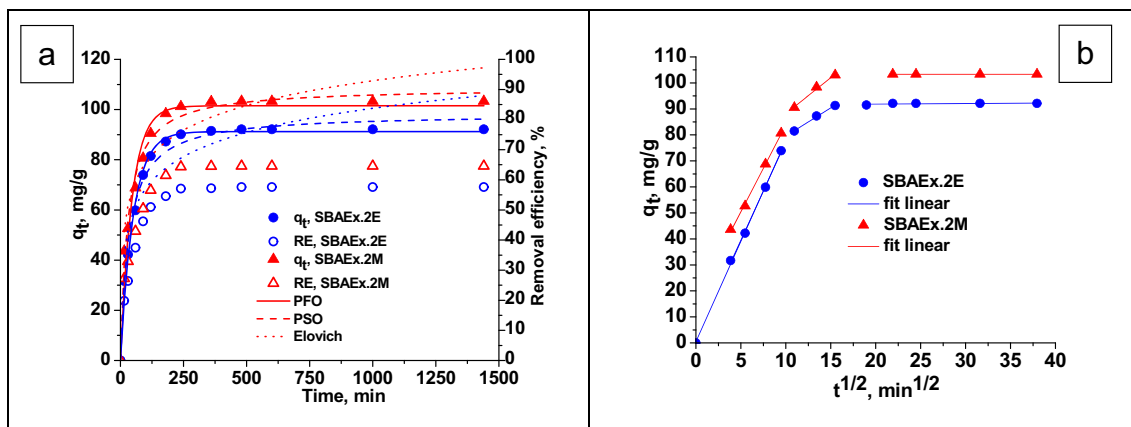


Fig. 2 Sorption kinetics of phosphate onto SBAEx, fitted by a PFO, PSO, and Elovich kinetic models. **b** Weber and Morris; sorption conditions: sorbent dose 0.75 g L⁻¹; C_{in} = 100 mg L⁻¹; pH 3; temp. 23 °C

$$E = 1/(2\beta)^{1/2} \tag{3}$$

The values of $E > 40 \text{ kJ mol}^{-1}$ for both sorbents indicate chemisorption as the most probable mechanism of sorption. Unlike the Langmuir isotherm, the Temkin adsorption model assumes that the adsorption sites in the adsorbent are unequal and have different adsorption coefficients and adsorption energies (Klimaviciute et al. 2010). The values of R^2 for the Temkin isotherm were 0.9489 and 0.9575, for the SBAEx.2E and SBAEx.2M,

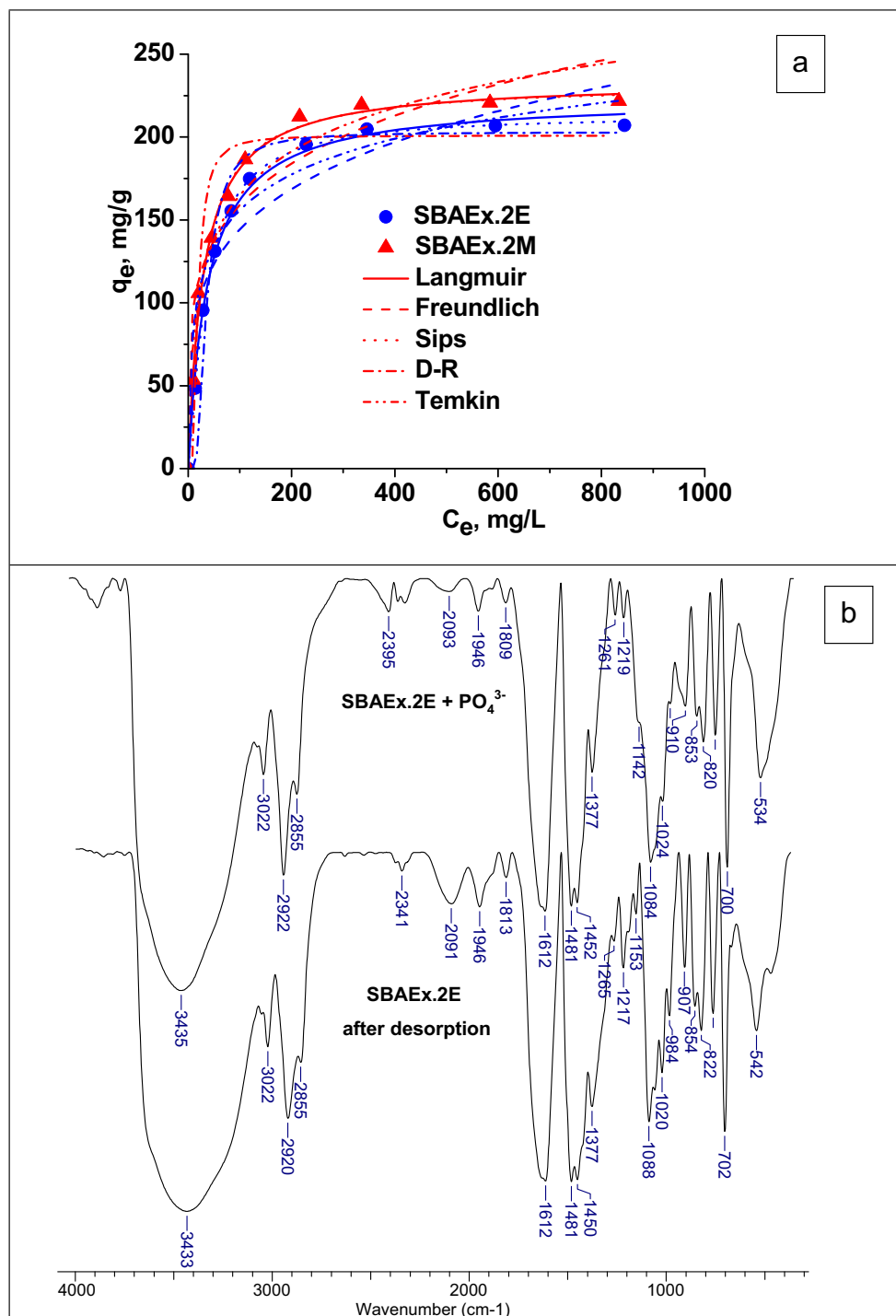
respectively. These values, besides the relatively low values of χ^2 , indicate a close fit of this isotherm to the sorption of phosphate anions.

The FTIR spectra of the SBAEx.2E after loading with phosphate and after desorption of phosphate anions are presented in Fig. 3b. The peak situated at 3435 cm^{-1} is assigned to $-\text{OH}$ stretching vibration; the peaks at 3022 cm^{-1} , 2922 cm^{-1} , and 2856 cm^{-1} correspond to $\text{C}-\text{H}$ and $-\text{CH}_2$ stretching vibrations. The peak located at 1481 cm^{-1} was assigned to aromatic $\text{C}-\text{C}$ stretch, while peak located at 1452 cm^{-1} was attributed to CH and CH_2 deformation vibrations. The

Table 2 Kinetic parameters for the adsorption of phosphate anions onto SBAEx, at 23 °C

Kinetic model	Parameters	Sorbent	
		SBAEx.2E	SBAEx.2M
	$q_{\text{exp}}, \text{ mg g}^{-1}$	92.13	103.31
PFO $q_t = q_e (1 - e^{-k_1 t})$	$q_e, \text{ calc.}, \text{ mg g}^{-1}$	91.21	101.49
	$k_1, \text{ min}^{-1}$	0.0198	0.0221
	R^2	0.9903	0.9687
	χ^2	8.47	31.86
PSO $q_t = \frac{k_2 q_e^2 t}{1 + k_2 q_e t}$	$q_e, \text{ calc.}, \text{ mg g}^{-1}$	98.4	108.72
	$k_2, \text{ g mg}^{-1} \text{ min}^{-1}$	3.0898×10^{-4}	3.292×10^{-4}
	R^2	0.9878	0.9874
	χ^2	10.68	12.8
Elovich $q_t = \frac{1}{\beta} \ln(1 + \alpha \times \beta \times t)$	$\alpha, \text{ mg g}^{-1} \text{ min}^{-1}$	19.14	36.21
	$\beta, \text{ g mg}^{-1}$	0.0719	0.0704
	R^2	0.9122	0.9314
	χ^2	77	70
IPD $q_t = k_{\text{id}} \times t^{0.5} + C_i$	$k_{\text{id},1}, \text{ mg g}^{-1} \text{ min}^{-0.5}$	7.727	6.675
	$C_1, \text{ mg g}^{-1}$	0.4463	17.046
	R_1^2	0.9991	0.9972
	$k_{\text{id},2}, \text{ mg g}^{-1} \text{ min}^{-0.5}$	2.17	2.77
	$C_2, \text{ mg g}^{-1}$	57.85	60.44
	R_2^2	0.9951	0.9796

Fig. 3 **a** Sorption isotherms of phosphate onto SBAEx. **b** FTIR spectra of SBAEx.2E after loading with phosphate and after phosphate desorption



adsorption bands located at 819, 761, and 700 cm^{-1} are assigned to the presence of p-substituted benzene rings (Coates 2000). The P–O stretching region is mentioned in literature as a band at 1000–1100 cm^{-1} (Li et al. 2019; Liao et al. 2020). In the case of SBAEx.2E, the in-plane deformation of aromatic CH overlapped the new peaks. However, the high adsorption of phosphate anions is supported by the following spectral features: the shoulder present at 1142 cm^{-1} in

the spectrum of SBAEx.2E, after loading with phosphate (Ding et al. 2012; Dragan et al. 2019; Liao et al. 2020), which disappeared after the removal of phosphate, while a peak can be observed at 1153 cm^{-1} . Also, the peak from 1084 cm^{-1} was shifted at 1088 cm^{-1} . In the case of SBAEx.2M, the peak characteristic for phosphate was identified at 1148 cm^{-1} , while a peak visible after desorption was located at 1073 cm^{-1} (spectra not shown here).

Table 3 Isotherm parameters for the adsorption of phosphate anions onto SBAEx, at 23 °C

Isotherm model	Parameters	Sorbent	
		SBAEx.2E 207	SBAEx.2M 221.65
Langmuir $q_e = q_m K_L \frac{C_e}{1+K_L C_e}$	$q_m, \text{mg g}^{-1}$	223.5	233.88
	$K_L, \text{L mg}^{-1}$	0.0264	0.0344
	R^2	0.9946	0.9953
	χ^2	28.4	28.3
	$q_{e,\text{exp}}, \text{mg g}^{-1}$		
Freundlich $q_e = K_F C_e^{1/n}$	$q_e, \text{mg g}^{-1}$	51.45	60.45
	$K_F, \text{mg}^{1-1/n} \text{L}^{1/n} \text{g}^{-1}$	0.224	0.2101
	R^2	0.8952	0.9076
	χ^2	0.555	556
	$q_m, \text{mg g}^{-1}$	213.55	232.64
Sips $q_e = q_m \frac{a_S C_e^{1/n}}{1+a_S C_e^{1/n}}$	a_S	0.0122	0.0321
	$1/n$	1.2355	1.0236
	R^2	0.9989	0.9947
	χ^2	5.78	32
	$q_{\text{DR}}, \text{mg g}^{-1}$	202.97	200.87
D-R $q_e = q_{\text{DR}} \exp\left\{-\beta \left[RT \ln\left(1 + \frac{1}{C_e}\right)\right]^2\right\}$	$\beta, \text{mol}^2 \text{kJ}^{-2}$	1.59264×10^{-4}	4.366×10^{-5}
	$E, \text{kJ mol}^{-1}$	56.03	107
	R^2	0.9204	0.8941
	χ^2	105	637
	$a_T, \text{L mg}^{-1}$	1.49	0.7562
Temkin $q_e = \frac{RT}{b_T} \ln a_T C_e$	$b_T, \text{J mol}^{-1}$	78.17	63.86
	R^2	0.9047	0.9575
	χ^2	125	256

To demonstrate the potential of the SBAEx.2M and SBAEx.2E as adsorbents for the phosphate anions, their maximum sorption capacities are compared in Table 4 with the values reported in literature for other sorbents.

As can be seen, the highest sorption capacities were reported for some composite sorbents, such as Zr-loaded IPN chitosan/PVA (Wan et al. 2017), alginate-Zr⁴⁺ and PNIPAM IPN (Luo et al. 2019), chitosan-PEI double network cryogels (Dragan et al. 2019), and for a quaternized resin based on AN/DVB/VBC matrix (Sowmya and Meenakshi 2014). As Table 4 shows, the SBAEx.2M and SBAEx.2E present superior adsorption performances, which recommend them as alternative for phosphate anion removal.

Thermodynamics

The values of the distribution coefficient (K_d), calculated with Eq. 4 at four temperatures: 293.15, 303.15, 313.15, and 323.15 K, were used to evaluate the thermodynamic parameters (ΔG° , ΔH° , and ΔS°) as reported for other adsorption systems (Granados-Correa and Jiménez-Reyes 2013; Guo et al. 2015; Kumar et al. 2013; Lu et al. 2019).

$$K_d = \frac{q_e}{C_e} \times M_{\text{adsorbate}} \tag{4}$$

where q_e is the amount of phosphate anions retained at equilibrium, mg g^{-1} , C_e is the concentration of phosphate at equilibrium, in the aqueous phase, mg L^{-1} , and $M_{\text{adsorbate}}$ is the mass of phosphate.

The units of K_d in Eq. 4 are L mol^{-1} . For the calculation of the thermodynamic parameters, K_d should be dimensionless. To solve this problem, the values of K_d were multiplied with 55.5 mol L^{-1} (Lütke et al. 2019), the obtained value being denoted with K° .

The values of enthalpy change (ΔH°) and entropy change (ΔS°) were evaluated using Van't Hoff equation (Eq. 5) from the slope and intercept of the plot $\ln K^\circ$ vs. $1/T$ (Fig. 4):

$$\ln K^\circ = \frac{\Delta S^\circ}{R} - \frac{\Delta H^\circ}{RT} \tag{5}$$

The change in the standard Gibbs free energy, ΔG° , was calculated with Eq. 6:

$$\Delta G^\circ = -RT \ln K^\circ \tag{6}$$

Table 4 Comparison of maximum equilibrium sorption capacity of phosphate anions on different sorbents

Sorbent	T, °C	Sorbent dose, g L ⁻¹	Initial pH	q _m , mg g ⁻¹	Ref.
SBAEx.2M	23	0.75	3	233.88	This study
SBAEx.2E	23	0.75	3	223.5	This study
Cross-linked chitosan	20	0.25	8.5	52.1	[9]
Fe-loaded chitosan-alginate hybrid beads	30	2	6	84.74	[10]
Humic acid-coated magnetic nanoparticles	25	10	6.6	28.9	[15]
Zr-loaded IPN chitosan/PVA	22	0.25	6.5	44.21 ^a	[17]
Magnetic Zr-alginate beads	25	2.5	2	42.23 ^a	[18]
Alginate-Zr ⁴⁺ and PNIPAM IPN	25	2.5	2	47.45 ^a	[19]
La-modified platanus biochar	35	0.4	6	148.11	[21]
Chitosan-PEI double network cryogels	25	0.75	3	343	[23]
Magnetic alginate hybrid beads	30	2	7	30.16	[24]
WSC-g-PKA/PVA semi-IPN	20	1	7.0	118.5	[25]
Magnetic ion exchanger	15	n.a.	n.a.	26.5	[26]
Quaternized resin based on AN/DVB/VBC matrix		2	4.9	183.18	[27]
Strong basic anion exchanger gel-type	25	0.1	7	12.47	[28]
Varian ATM	20	1.5	5	66.22	[29]

^a mg P; n.a. not available

The values of all thermodynamic parameters are presented in Table 5.

The negative values of ΔG° show that the sorption process was spontaneous and the increase of the negative value with the increase of temperature supports the increase of the degree of spontaneity for the sorption of phosphate anions onto both anion exchangers. The positive values of ΔH° show that the sorption process was endothermic, and the positive values of ΔS° indicate the increase of the randomness at the solid-liquid interface.

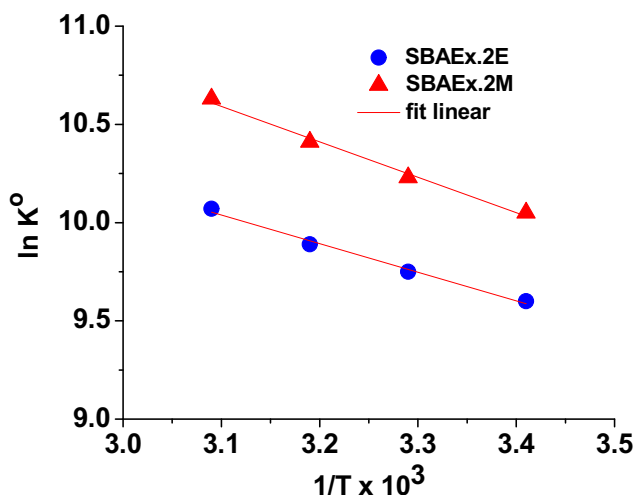


Fig. 4 Plot of $\ln K^\circ$ versus $1/T$ for the sorption of phosphate onto SBAEx; sorbent dose 0.75 g L⁻¹, pH 3, $C_{in} = 100$ mg L⁻¹, contact time 12 h

Effect of interfering anions and reusability

Adsorption in competitive conditions

To evaluate the influence of coexisting anions on the phosphate removal by SBAEx.2M and SBAEx.2E, the sorption study was conducted in the presence of three competing anions: Cl^- , NO_3^- , and SO_4^{2-} , which usually are present in the wastewaters containing phosphate anions (Du et al. 2020; Hao et al. 2019; Karthikeyan et al. 2019; Luo et al. 2019; Liu et al. 2013; Sowmya and Meenakshi 2014). Figure 5a shows that the interference of coexisting anions with phosphate was the highest for SO_4^{2-} and the lowest for Cl^- , increasing with the increase of anion concentration.

Thus, the sorption capacity decreased from 91.85 to 71.56 mg g⁻¹ in the case of SBAEx.2M, and from 80.63 to 55.34 mg g⁻¹ in the case of SBAEx.2E, when the concentration of NaCl increased from 0.001 to 0.1 M (the initial sorption capacity was 103.31 mg g⁻¹ for SBAEx.2M and 92.13 mg g⁻¹ for SBAEx.2E). Compared with Cl^- ions, the competition of SO_4^{2-} anions with H_2PO_4^- ions was much stronger because these are divalent ions, the level of interference with NO_3^- being in the middle (Karthikeyan et al. 2019). Results presented in Fig. 5a show that the SBAEx.2M at least could be successfully used in the removal of phosphate anions even in the presence of interfering anions.

Reusability

To evaluate the reusability of the SBAEx under investigation, five consecutive sorption/desorption cycles were

Table 5 Thermodynamic parameters for the sorption of phosphate onto SBAEx.2M and SBAEx.2E

Sorbent	ΔH° , kJ mol ⁻¹	ΔS° , kJ mol ⁻¹ K ⁻¹	ΔG° , kJ mol ⁻¹			
			293.15	303.15	313.15	323.15
SBAEx.2M	12.12	0.121	- 23.35	- 24.56	- 25.77	- 26.98
SBAEx.2E	15.00	0.135	- 24.58	- 25.93	- 27.28	- 28.63

performed (Fig. 5b). The decrease of the adsorption capacity for phosphate after five cycles was of 7.35% in the case of SBAEx.2E and 9.13% in the case of SBAEx.2M, and the results support great potential for these porous anion exchangers in the removal of phosphate ions.

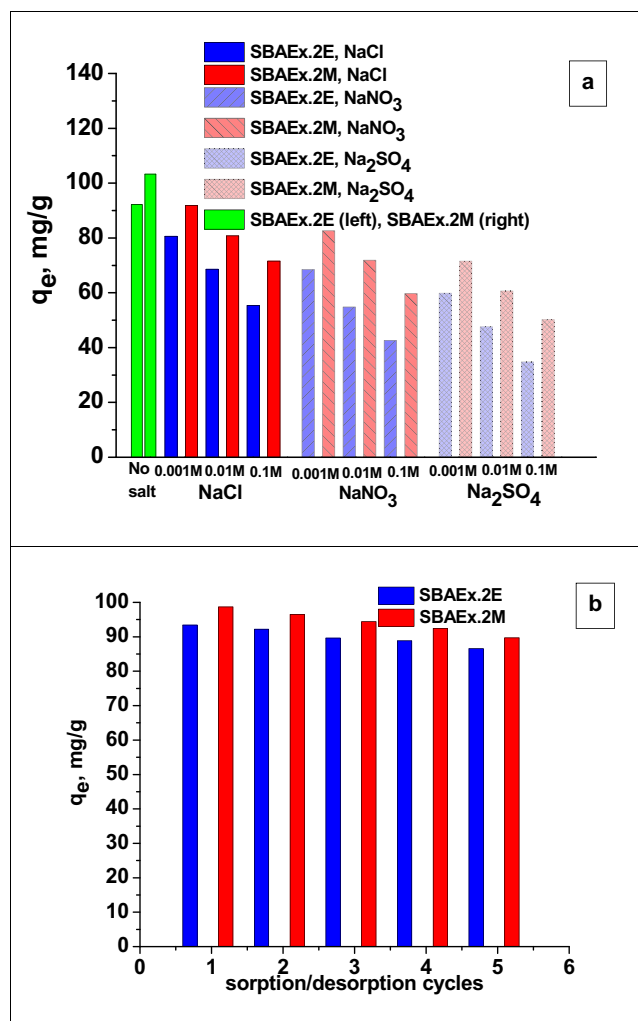


Fig. 5 a Competitive sorption of phosphate onto SBAEx in presence of interfering co-ions. b Evaluation of phosphate sorption capacity as a function of sorption/desorption cycles: sorbent dose 0.75 g L⁻¹; C_{in} = 100 mg L⁻¹; eluent 4 wt.% NaCl

Conclusions

The analysis of the results presented in the paper has conducted to the following conclusions:

- Sorption of phosphate anions onto the SBAEx having N,N-dialkyl 2-hydroxyethyl ammonium groups was higher when the substituents were methyl than ethyl, and this shows that the ion exchange had the most important contribution in the phosphate uptake;
- Chemisorption had an important contribution demonstrated by the sorption kinetics and by the high values of mean free energy of adsorption (56 kJ mol⁻¹ for SBAEx.2E and 107 kJ mol⁻¹ for SBAEx.2M);
- The sorption at equilibrium was well fitted by the Langmuir and Sips isotherms supporting monolayer adsorption, irrespective of the alkyl substituents;
- The more hydrophobic alkyl substituents seem to be beneficial for the life expectancy of the anion exchanger during the multiple sorption/desorption cycles, the decrease of the sorption capacity being lower in the case of SBAEx.2E than for SBAEx.2M, after five sorption/desorption cycles.

Authors’ contributions DH performed the adsorption experiments of phosphate on anion exchangers. ESD synthesized and characterized the anion exchangers, writing and editing the paper. Both authors read and approved the final manuscript.

Funding This research did not receive any specific grant from funding agencies in the public, commercial, or non-for-profit sectors.

Data availability The datasets used and/or analysed during the current study are available from the corresponding author on reasonable request.

Compliance with ethical standards

Competing interest The authors declare that they have no competing interest.

Ethics approval and consent to participate Not applicable.

Consent for publication Not applicable.

References

- Azam HM, Alam ST, Hasan M, Yameogo DDS, Kannan AD, Rahman A, Kwon MJ (2019) Phosphorus in the environment: characteristics with distribution and effects, removal mechanisms, treatment technologies, and factors affecting recovery as minerals in natural and engineered systems. *Environ Sci Pollut Res* 26:20183–20207
- Bassin JP, Kleerebezem R, Dezotti M, van Loosdrecht MCM (2012) Simultaneous nitrogen and phosphate removal in aerobic granular sludge reactors operated at different temperatures. *Water Res* 46:3805–3816
- Bui TH, Hong SP, Yoon J (2018) Development of nanoscale zirconium molybdate embedded anion exchange resin for selective removal of phosphate. *Water Res* 134:22–31
- Bunce JT, Ndam E, Ofiteru ID, Moore A, Graham DW (2018) A review of phosphorus removal technologies and their applicability to small-scale domestic wastewater treatment systems. *Front Environ Sci* 6:1–15
- Coates J (2000) Interpretation of infrared spectra, a practical approach. In: Meyers RA (ed) *Encyclopedia of Analytical Chemistry*. John Wiley & Sons Ltd, Chichester, pp 10815–10837
- Ding L, Wu C, Deng H, Zhang X (2012) Adsorptive characteristics of phosphate from aqueous solutions by MIEIX resin. *J Colloid Interface Sci* 376:224–232
- Dragan S, Cristea M, Airinei A, Luca C, Ig P (1995) Sorption of aromatic compounds on macroporous anion-exchangers based on polyacrylamide - relation between structure and sorption behavior. *J Appl Polym Sci* 55:421–430
- Dragan ES, Dinu MV (2020) Advances in porous chitosan-based composite hydrogels: synthesis and applications. *React Funct Polym* 146:Nr. 104372
- Dragan ES, Humelnicu D, Dinu MV (2018) Design of porous strong base anion exchangers bearing N,N-dialkyl 2-hydroxyethyl ammonium groups with enhanced retention of Cr(VI) ions from aqueous solution. *React Funct Polym* 124:55–63
- Dragan ES, Humelnicu D, Dinu MV (2019) Development of chitosan-poly(ethyleneimine) based double network cryogels and their applications as superadsorbents for phosphate. *Carbohydr Polym* 210:17–25
- Du J, Dong Z, Yang X, Zhao L (2020) Radiation grafting of dimethylaminoethyl methacrylate on cotton linter and subsequent quaternization as new eco-friendly adsorbent for phosphate removal. *Environ Sci Pollut Res* 27:24558–24567
- Granados-Correa F, Jiménez-Reyes M (2013) Kinetic, equilibrium and thermodynamic studies on the adsorption of Eu(III) by eggshell from aqueous solutions. *Adsorpt Sci Technol* 31:891–902
- Guo Z, Liu X, Huang H (2015) Kinetics and thermodynamics of reserpine adsorption onto strong acidic cationic exchange fiber. *PLoS One* 10:e0138619
- Hao H, Wang Y, Shi B (2019) NaLa(CO₃)₂ hybridized with Fe₃O₄ for efficient phosphate removal: synthesis and adsorption mechanistic study. *Water Res* 155:1–11
- Ho YS, McKay G (1998) The kinetics of sorption of basic dyes from aqueous solution by sphagnum moss peat. *Can J Chem Eng* 76:822–827
- Jia Z, Zeng W, Xu H, Li S, Peng Y (2020) Adsorption removal and reuse of phosphate from wastewater using a novel adsorbent of lanthanum-modified platanus biochar. *Process Saf Environ Prot* 140:221–232
- Jing X, Chen L, Wang Y, Wang Y, Yang X, Dai J, Dai X, Jiang Y, Liu Y, Liu Z, Yan Y (2020) Efficient removal of phosphate with La modified rGO/silica large mesoporous films. *J Taiwan Inst Chem Eng* 111:170–180
- Juang RS, Chen ML (1997) Application of the Elovich equation to the kinetics of metal sorption with solvent-impregnated resins. *Ind Eng Chem Res* 36:813–820
- Karthikeyan P, Thagira Banu HA, Meenakshi S (2019) Synthesis and characterization of metal loaded chitosan-alginate biopolymeric hybrid beads for the efficient removal of phosphate and nitrate ions from aqueous solution. *Int J Biol Macromol* 130:407–418
- Klimaviciute R, Bendoraitiene J, Rutkaite R, Zemaitaitis A (2010) Adsorption of hexavalent chromium on cationic cross-linked starches of different botanic origins. *J Hazard Mater* 181:624–632
- Kumar A, Rout S, Ghosh M, Singhal RK, Ravi PM (2013) Thermodynamic parameters of U(VI) sorption onto soils in aquatic systems. *SpringerPlus* 2:530
- Kumar IA, Viswanathan N (2018) Preparation and testing of a tetra-amine copper(II) chitosan bead system for enhanced phosphate remediation. *Carbohydr Polym* 183:173–182
- Kumar IA, Viswanathan N (2019) Micro-encapsulation and hydrothermal tuning of amine decorated magnetic alginate hybrid beads for nitrate and phosphate remediation. *J Taiwan Inst Chem Eng* 102:283–296
- Lagergren S (1898) *Kungliga Svenska Vetenskapsakademien Handlingar*. 24:1–39
- Li T, Huang P, Liao T, Guo J, Yu X, Han B, Peng L, Zhu Y, Zhang Y (2019) Magnetic polymer-supported adsorbent with two functional adsorption sites for phosphate removal. *Environ Sci Pollut Res* 26:33269–33280
- Liao T, Huang P, Song H, Guo J, Fu X, Yu X, Peng L, Han B, Zhu Y, Zhang Y (2020) La(OH)₃-modified magnetic sodium carboxymethyl cellulose for sequential removal of pollutants: adsorption of phosphate and subsequent photocatalytic reduction of Cr(VI). *Environ Sci Pollut Res*, just accepted
- Liu J, Su Y, Li Q, Yue Q, Gao B (2013) Preparation of wheat straw based superabsorbent resins and their applications as adsorbents for ammonium and phosphate removal. *Bioresour Technol* 143:32–39
- Liu J, Wan L, Zhang L, Zhou Q (2011) Effect of pH, ionic strength, and temperature on the phosphate adsorption onto lanthanum-doped activated carbon fiber. *J Colloid Interface Sci* 364:490–496
- Lu S, Chen L, Hamza MF, He C, Wang X, Wei Y, Guibal E (2019) Amidoxime functionalization of a poly(acrylonitrile)/silica composite for the sorption of Ga(III) – application to the treatment of Bayer liquor. *Chem Eng J* 368:459–473
- Luo H, Rong H, Zhang TC, Zeng X, Wan J (2018) Amino-functionalized magnetic zirconium alginate beads for phosphate removal and recovery from aqueous solutions. *J Appl Polym Sci* APP.46897
- Luo H, Zeng X, Liao P, Rong H, Zhang TC, Zhang ZJ, Meng X (2019) Phosphorus removal and recovery from water with macroporous bead adsorbent constituted of alginate-Zr⁴⁺ and PNIPAM interpenetrated networks. *Int J Biol Macromol* 126:1133–1144
- Lütke SF, Igansi AV, Pegoraro L, Dotto GL, Pinto LLA, Cadaval TRS Jr (2019) Preparation of activated carbon from black wattle bark waste and its application for phenol adsorption. *J Environ Chem Eng* 7:103396
- Mahaninia MH, Wilson LD (2016) Cross-linked chitosan beads for phosphate removal from aqueous solution. *J Appl Polym Sci* 133:APP.42949
- Mahaninia MH, Wilson LD (2017) Phosphate uptake studies of cross-linked chitosan bead materials. *J Colloid Interface Sci* 485:201–212
- Nagul EA, McKelvie ID, Worsfold P, Kolev SD (2015) The molybdenum blue reaction for the determination of orthophosphate revisited: opening the black box. *Anal Chim Acta* 890:60–82
- Nassef E (2012) Removal of phosphates from industrial waste water by chemical precipitation. *Eng Sci Technol Int J* 2:409–413
- Rashid M, Price NT, Pinilla MAG, O'Shea KE (2017) Effective removal of phosphate from aqueous solution using humic acid coated magnetite nanoparticles. *Water Res* 123:353–360

- Sowmya A, Meenakshi S (2014) A novel quaternized resin with acrylonitrile/divinylbenzene/vinylbenzyl chloride skeleton for the removal of nitrate and phosphate. *Chem Eng J* 257:45–55
- Wan J, Zhu C, Hu J, Zhang TC, Richter-Eggerd D, Feng X, Zhou A, Tao T (2017) Zirconium-loaded magnetic interpenetrating network chitosan/poly(vinyl alcohol) hydrogels for phosphorus recovery from the aquatic environment. *Appl Surf Sci* 423:484–491
- Weber JWJ, Morris JC (1963) Kinetics of adsorption on carbon from solution. *J San Eng Div Proceed Am Soc Civ Eng* 89:31–60
- Wei LL, Wang GZ, Jiang JQ, Li G, Zhang XL, Zhao QL, Cui FY (2015) Co-removal of phosphorus and nitrogen with commercial 201 × 7 anion exchange resin during tertiary treatment of WWTP effluent and phosphate recovery. *Des Water Treat* 56:1633–1647
- Wu K, Li Y, Liu T, Zhang N, Wang M, Yang S, Wang W, Jin P (2019) Evaluation of the adsorption of ammonium-nitrogen and phosphate on a granular composite adsorbent derived from zeolite. *Environ Sci Pollut Res* 26:17632–17643
- Ye Y, Jiao J, Kang D, Jiang W, Kang J, Ngo HH, Guo W, Liu Y (2019) The adsorption of phosphate using a magnesia–pullulan composite: kinetics, equilibrium, and column tests. *Environ Sci Pollut Res* 26:13299–13133
- Zarrabi M, Soori MM, Sepehr MN, Amrane A, Borji S, Ghaffari HR (2014) Removal of phosphorus by ion exchange resins: equilibrium, kinetic and thermodynamic studies. *Environ Eng Manag J* 13:891–903
- Zhao D, Chen JP (2016) Application of zirconium/PVA modified flat-sheet PVDF membrane for removal of phosphate from aqueous solution. *Ind Eng Chem Res* 55:6835–6844
- Zhu C, Wang Q, Pang W, Wang Z, Cao J, Hu W, Tang J, Huang J, Wu Z (2017) Mechanism of phosphorus removal from wastewater by ion exchange resin. *Des Water Treat* 79:347–355
- Zong E, Huang G, Liu X, Lei W, Jiang S, Ma Z, Wang J, Song P (2018) A lignin-based nano-adsorbent for superfast and highly selective removal of phosphate. *J Mater Chem A* 6:9971–9983

Publisher's note Springer Nature remains neutral with regard to jurisdictional claims in published maps and institutional affiliations.